Modelling of the Shear Dilation Based Hydraulic Stimulation in Enhanced Geothermal Systems Considering Fractures in Different Scales

Eren Ucar[1], Inga Berre[1], Eirik Keilegavlen[1]

[1] Department of Mathematics, University of Bergen, 5020 Bergen, Norway

eren.ucar@uib.no

Keywords: numerical simulation, discrete fracture matrix model, hydraulic stimulation, soft stimulation, shear dilation, matrix permeability.

ABSTRACT

A numerical approach for modelling of shear dilation of existing fractures in hydraulic stimulation of geothermal reservoirs at low elevated pressures is presented.

The fractured rock in the reservoir is modelled as a combination of explicitly represented fractures and the rock matrix surrounding these fractures. The efficient modelling of slip-induced permeability enhancement requires coupling of the fluid flow in fractured rock with the mechanical deformation of the rock matrix and the shear dilation of the fractures. For flow simulations, conductive fractures are represented in the domain as high-permeable discontinuities; therefore they dominate the overall flow behaviour. The rock matrix is represented by a low permeability, capturing the effect of small-scale fractures. For the mechanical deformation problem, the rock matrix is assumed to be a linear elastic material, while the fractures in the rock matrix are introduced as internal boundaries. The shear dilation of the fractures is calculated by a joint deformation model (JDM), which connects the shear slip in the fracture surfaces and additional permeability caused by shear displacement. The flow simulations and the mechanical deformation of the rock matrix are both obtained by finite volume discretizations.

Several numerical experiments designed by resembling realistic reservoir parameters are conducted to provide better understanding of the shear dilation mechanism. Moreover, fractures present in different scales in a geothermal reservoir. Ignoring the effect of small-scale fractures to the fluid flow in the matrix may result in an overestimate of the permeability enhancement. Hence, the influence of rock matrix permeability on fracture aperture and the overall flow behaviour of the reservoir are examined.

1. INTRODUCTION

Enhanced Geothermal Systems (EGS) can facilitate increased heat production from low-permeable rocks, and thus make geothermal resources where natural permeability is inadequate commercially viable. The permeability enhancement in EGS can be created by three main stimulation methods, as hydraulic, chemical and thermal stimulation. The most commonly used method is hydraulic stimulation (Breede et al. 2013). Two main approaches to hydraulic stimulation are denoted hydraulic fracturing and shear dilation stimulation (a.k.a. shear stimulation, hydroshearing or low-pressure stimulation). Hydraulic fracturing involves the injection of fluid at a high pressure to overcome the minimum principal stress. In this method, fractures are initiated and propagated by induced fluid pressure and commonly retained by proppants. However, Zhang et al. (1997) has shown that hydraulic fracturing is not efficient enough for formations where the differences between maximum and minimum horizontal in-situ stresses are large and natural fractures already exist. In these reservoirs, shear dilation of fractures has been identified as the dominant mechanism responsible for the enhancement of permeability (Pine and Batchelor 1984, Murphy and Fehler 1986). Shear dilation stimulation is performed by elevating fluid pressures in pre-existing fractures in low permeability rock. As opposed to hydraulic fracturing, the injection pressures are below the minimum in situ principle stress of the reservoir, but above the threshold required for shearing of fractures. The increase in fluid pressure reduces the normal force on the fracture surfaces, allowing them to slip and dilate. The shear dilation in the fracture surfaces leads to a permeability enhancement since the asperities on the fracture walls slide over each other and resist the fracture surfaces sliding back.

The progression of EGS relies on the ability to predict how the reservoir will behave under the stimulation process. Therefore, there is a need for a reliable reservoir simulation model. There have been a number of worthwhile modelling studies in the relevant literature from modelling of individual fracture deformation (Barton et al. 1985, Barton and Choubey 1977) to simulations including the effect of several fractures on larger scale domains (Willis-Richards et al. 1996, Jing et al. 2000, Rahman et al. 2002, Min et al. 2004, Tezuka et al. 2005, Bruel 2007, Tao et al. 2011, McClure and Horne 2011, McClure and Horne 2014, Norbeck et al. 2016). Modelling studies related

to shear stimulation of EGS are challenging due to several reasons, of which we emphasize three: 1) Although natural fractures can occur on all scales, the domain is generally modelled either as a combination of fractures and impermeable surrounding rock, or using an approximated continuum model to represent the flow properties of the fracture network. This will have the effect of respectively over- or underestimating fluid pressure in the fracture. 2) Coupling of flow, mechanical deformation and fracture deformation in fractured porous media, is challenging both from a modelling and from a numerical perspective. 3) As the elastic properties of a geothermal reservoir may not be homogenous, several numerical approaches have limitations.

In this study, the effect of multiscale fractures is handled by applying a discrete fracture matrix (DFM) model (Karimi-Fard et al. 2004), wherein the fractures that constitute the main flow paths are explicitly represented, while smaller scale fractures are represented by an averaged matrix permeability. The DFM model provides avoiding inaccurate approximation of permeability increase due to the wrong pressure estimations.

In the related literature, the simulation strategies generally rely on coupling different numerical discretization methods for two individual problems. The flow problems were generally treated by finite volume discretization (Chen et al. 2006) whereas the mechanical problem was most commonly solved either by finite element discretization (Jha and Juanes 2014, Garipov et al. 2015) or an indirect boundary element method (Crouch and Starfield 1983, McClure and Horne 2011, McClure and Horne 2014, Norbeck et al. 2016) called displacement discontinuity method (DDM). Using different discretization for flow and mechanics problems requires additional coupling strategies (Kim et al. 2011) and different data structures. Moreover, DDM has limitations regarding to boundary conditions, being not suitable to implement heterogonous elastic properties and restriction to two-dimensional analysis. Therefore, for both flow and mechanics problem, cell-centred finite volume discretization is used in this study. In this study, the fluid flow is modelled by two-point flux approximation (TPFA) whereas mechanical behaviour of fractured rock matrix is handled by the multi-point stress approximation (MPSA). MPSA was proposed recently as a compatible counterpart to finite-volume flow calculations in porous media (Nordbotten 2014). MPSA is further extended effectively to allow for inclusion of fractures through internal boundary conditions in the discretization (Ucar et al. draft manuscript), which naturally enables the implementation of fracture deformation in the present study. Moreover, MPSA provides to include the effect of possible heterogeneities in the elastic properties however that is not yet the scope of the current study.

The main purpose of the current work is to provide efficient modelling of shear dilation stimulation for EGS. The model equations and coupling scheme are presented in Section 2. The numerical approach used in this study is described in Section 3. Section 4 shows a detailed numerical example of simulation strategy based on realistic reservoir parameters. Moreover, we want to stress the effect of permeability in the regions surrounding the explicitly modelled fractures. A numerical example that shows the effect of the matrix permeability is, hence, also provided in this section. Finally, conclusions and comments related to further work are given in Section 5.

2. GOVERNING EQUATIONS

In this section, we introduce the governing equations to model low-pressure stimulation in a fractured porous domain, such as EGS systems. Before presentation of the modelling equations, let Ω be our domain of interest and $\partial\Omega$ be its boundary. The modelling includes coupling of fluid flow, mechanical deformation and a constitutive relation for permeability enhancement in the considered domain. Therefore, conservation equations for mass and momentum for both rock matrix and fractures are presented. Moreover, the joint deformation model, which is used to estimate resulting permeability evolution caused by deformation, is presented.

2.1 Conservation of Mass

The fractured rock in the reservoir is considered as a porous media that includes high permeable slit-like discontinuities, namely fractures. In this study, it is assumed that the fractured porous domain is stimulated by injecting an isothermal, single-phase, slightly compressible fluid at elevated pressures. Under these assumptions, the mass balance equation for fluid can be written as

$$\partial m/\partial t+\nabla\cdot(\rho_f \mathbf{w}) = q. \qquad [1]$$

The time derivative term in equation [1] represents mass accumulation in a control volume where m is fluid mass and ρ_f is the fluid density. q stands for the source terms and the Darcy flux, $\mathbf{w}$, can be calculated by introducing Darcy's law without gravity vector:

$$\mathbf{w} = -\mathbf{K}/\eta\,(\nabla p), \qquad [2]$$

where $\mathbf{K}$, η and p are intrinsic permeability of porous media, dynamic viscosity of fluid, pore fluid pressure, respectively.

Combining equation [1] and [2] leads to the mass conservation equation for single-phase flow of a slightly compressible fluid. Note that the time derivative term in equation [1] can be written as

$$\partial m/\partial t = \phi c_t\, \partial p/\partial t, \qquad [3]$$

where ϕ is porosity, assuming that the fluid compressibility is small and constant. The total compressibility, c_t, is sum of fluid compressibility, c, and pore-volume compressibility, c_f.

The discrete fracture matrix (DFM) model (Karimi-Fard et al. 2004, Sandve, et al. 2012) provides the basic conceptual model in the present study. In DFM models, explicitly represented fractures are combined with an effective low permeability tensor defined in the surrounding porous medium (the porous medium excluding big scale fractures) to capture flow in pores and small-scale fractures not represented explicitly. Then by assuming the fracture surfaces are smooth parallel walls separated by a uniform aperture, e, the permeability of the explicitly modelled fractures can be calculated by the 'cubic law' (Jaeger 2007):

$$K = e^2/12, \qquad [4]$$

According to several studies (Barton et al. 1985, Chen et al. 2000, Olsson and Barton 2001), the void between fracture surfaces, mechanical aperture, can be different then hydraulic aperture. In reality, the hydraulic aperture between fracture surfaces depends on several parameters such as roughness, tortuosity or contacts between the fracture surfaces (Zimmerman and Bodvarsson 1996). In this study, we ignore this inequality, however it can be easily be included in our approach.

2.2 Linear Momentum Balance

The considered problem is assumed to be quasi-static, thus the inertial effect and time dependence can be ignored. Under the quasi-static assumption, the stresses induced by fracture slip can be calculated by using equation for linear momentum balance of an elastic medium as

$$\nabla \cdot \boldsymbol{\sigma} = 0, \qquad [5]$$

where $\boldsymbol{\sigma}$ is the Cauchy stress tensor. In addition, we assume a linear relation between strain and stress through Hooke's law,

$$\boldsymbol{\sigma} = \mathbb{C} : \boldsymbol{\varepsilon}, \qquad [6]$$

where $\mathbb{C}$ is the symmetric fourth-rank stiffness tensor and ε is the symmetric part of the displacement gradient tensor as

$$\boldsymbol{\varepsilon} = ((\nabla \mathbf{u} + (\nabla \mathbf{u})^T))/2, \qquad [7]$$

where $\mathbf{u}$ is the displacement of a point.

For an isotropic medium, one can write the symmetric fourth-rank stiffness tensor in terms of constants as μ and λ then obtain isotropic form of Hooke's law as

$$\boldsymbol{\sigma} = 2\mu\boldsymbol{\varepsilon} + \lambda \, \mathrm{tr}(\boldsymbol{\varepsilon}) \, \mathbf{I}. \qquad [8]$$

In equation [8], $\mathbf{I}$ is identity matrix. μ and λ are known as Lamé constants, μ being the shear modulus that relates shear stress to shear strain.

It is important to note that, we do not consider the effect of flow while solving the mechanics problem. We assume that the timescale of the mechanical deformation to be much shorter than one relevant for the flow. Any perturbation in the elastic domain, in the current case shear slip, immediately propagates across the whole domain. Similarly, motivated by the assumption of hard rocks, which are the common target formation for EGS operations, we ignore poro-elastic effects when solving the flow equation.

2.3 Mechanics of Fracture Deformation

In this study, the fracture surfaces are exposed to displacement discontinuities due to the pressure increase. We implement the deformation of the fractures through internal boundary conditions by using the method proposed by Ucar et al. (draft manuscript), which naturally allows defining displacement jumps between the fracture surfaces. In line with Aagaard et al. (2013), the fracture surfaces are considered as line pairs for 2D (faces for 3D) studies, which displaces relative to one another as illustrated in Figure 1. Following the notation for fracture surfaces from, for example, Aagaard et al. (2013) and Crouch and Starfield (1983), we denote two sides of discontinues by subscripts + and -. Slip at the fracture surfaces Γ can be defined as displacement of the '+' side relative to '-' side such as

$$\mathbf{u}_+ - \mathbf{u}_- = \mathbf{d} \text{ on } \Gamma, \qquad [9]$$

where $\mathbf{u}_+$ and $\mathbf{u}_-$ are the displacements on the positive and negative side fracture surfaces and $\mathbf{d}$ is displacement jump vector. The tractions on the fracture surfaces are continuous and satisfy equilibrium,

$$\mathbf{T}_+ - \mathbf{T}_- = 0 \text{ on } \Gamma, \qquad [10]$$

where the surface tractions are defined as

$$\boldsymbol{\sigma} \cdot \mathbf{n} = \mathbf{T}, \qquad [11]$$

for any surface has normal $\mathbf{n}$. The surface traction acting normal direction to a fracture surface represented as $\boldsymbol{\sigma}_\mathbf{n}$ and the surface traction acting tangential direction to a fracture surface represented as $\boldsymbol{\tau}$ in the following equations.

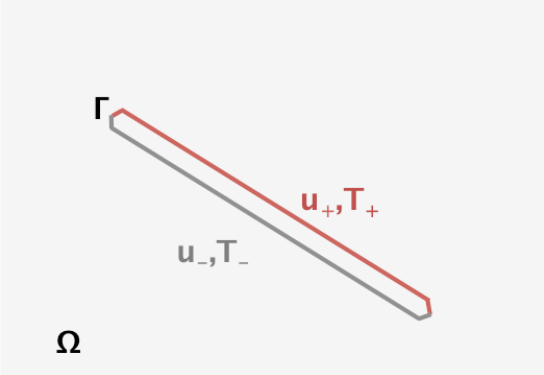

Figure 1: Fracture representation in a porous medium.

2.4 Fracture Deformation and Permeability Evolution (Joint Deformation Model)

Fractures in the rock matrix can be considered as planes of weaknesses in an elastic material and the stress conditions on these planes of weaknesses can be calculated for any given principal stresses (Jaeger et al. 2007).

In this study, we use Mohr- Coulomb theory to define the shear stability criterion for the fractures (Jaeger et al. 2007). The shear slip between the fracture surfaces occurs when the shear traction of the fractures is larger than the frictional resistance to slip (also called shear strength). The frictional resistance is a function of the material property of fractures and effective stress state. In the case of two rough surfaces sliding over one another with fluid in between, the effective normal thrust transmitted through the points of contact is

$$\boldsymbol{\sigma}_{\mathbf{eff}} = \boldsymbol{\sigma}_{\mathbf{n}} - P, \qquad [12]$$

where $\boldsymbol{\sigma}_{\mathbf{eff}}$, $\boldsymbol{\sigma}_{\mathbf{n}}$, P are effective stress, normal stress and pressure, respectively.

The frictional resistance can be decreased by elevating the fluid pressure inside of a pre-existing fracture by injection of fluid. When the pressure inside the fracture increases, the fluid in the fracture is pushing back opposite to the normal stress. Therefore, increasing fluid pressure in the fracture leads to shear displacement between fracture surfaces. When the asperities on opposite fracture surfaces slide over each other due to the shear displacement, the motion creates additional void due to aperture increase, called shear dilation. The shear dilation of fractures can be increased by increasing the pressure inside the fractures. However, the injection pressure can only be increased up to the limit of minimum principal stress. If the pressure inside the fractures exceeds the minimum principal stress, the fracture surfaces loose contact and the fracture then propagates along a plane perpendicular to the minimum principal stress direction. This phenomenon is known as conventional hydraulic fracturing and beyond the scope of this study. Therefore, the injection pressure is kept lower than minimum principal stress throughout the stimulation in the present work.

In the literature, there are documented numerous constitutive models for fracture behaviour under stress conditions (e.g. Barton et al. 1985, Willis-Richards et al.1996). In the current study, shear displacement and shear dilation based on normal and shear tractions of fractures are calculated following the procedure discussed by Willis-Richards et al. (1996). Based on the Mohr-Coulomb criterion, shear displacement occurs when the shear stress component acting parallel to the fracture surfaces is greater than shear strength of each fracture,

$$\boldsymbol{\tau} \geq \boldsymbol{\tau}_{\mathbf{p}}, \qquad [13]$$

where $\boldsymbol{\tau}_{\mathbf{p}}$ is the shear strength. In the model of Willis-Richards et al. (1996), the shear strength of each fracture can be calculated by using the Mohr-Coulomb criterion coupled with effective stresses and cohesive forces on the fracture,

$$\boldsymbol{\tau}_{\mathbf{p}} = \boldsymbol{\sigma}_{\mathbf{eff}} \tan(\phi_{basic} + \phi_{dil}^{eff}) + c, \qquad [14]$$

where c is cohesion, ϕ_{basic} is basic friction angle (a material property of the fractures, which typically alters between 30 and 40 (Willis-Richards et al.,1996)). The effective shear dilation angle, ϕ_{dil}^{eff}, is a property of both the fracture surface asperities and the normal stress, and may be written in terms of the laboratory measured shear dilation angle as

$$\phi_{dil}^{eff} = \phi_{dil}/(1+9(\boldsymbol{\sigma}_{\mathbf{eff}}/\boldsymbol{\sigma}_{\mathbf{nref}})), \qquad [15]$$

where ϕ_{dil} is dilation angle measured at zero, or at least at very low, effective stresses and $\boldsymbol{\sigma}_{\mathbf{nref}}$ is the effective normal stress applied to cause a 90% reduction in the compliant aperture.

The difference between shear strength and shear stress acting parallel to the fractures surface is denoted "excess" shear stress. The amount of shear displacement, $\mathbf{u}_{\mathbf{s}}$, can approximately be calculated by using relation between available "excess" shear stress, $\Delta\boldsymbol{\tau}$, and shear stiffness, K_s, based on linear elastic theory,

$$\mathbf{u}_{\mathbf{s}} = \Delta\boldsymbol{\tau}/K_s, \qquad [16]$$

where the shear stiffness, K_s, is a material property. The final aperture increase, $\mathbf{a}_{\mathbf{s}}$, due to shear displacement can be calculated by

$$\mathbf{a}_{\mathbf{s}} = \mathbf{u}_{\mathbf{s}} \tan(\phi_{dil}^{eff}). \qquad [17]$$

2.5 Boundary and Initial Conditions

To complete the model, initial and boundary conditions for both the flow and the mechanics problem must be defined. Constant pressure boundary condition is used for the flow equation while constant displacement boundary condition is used for the mechanics problem. The domain is extended enough to reduce spurious boundary effects for both flow and mechanics problem. Additionally, the initialization of the problem is carried out under the assumption of flow and mechanical equilibrium with constant pressure and zero displacement fields.

3. NUMERICAL IMPLEMENTATION

In this section, the numerical discretization of the equations given in Section 2 is presented. We start with the spatial discretization of conservation of mass and linear elasticity, including the fracture implementation. Thereafter, the time discretization and the solutions methods for the resulting system of equations are presented, respectively.

3.1 Grid Structure and Spatial Discretization

We apply finite volume discretizations for both the flow and the mechanics problem to ensure consistency

between the two. By using cell-centered discretization for both problems, we take advantage of having the primary unknowns (pressure for flow problem and deformation for mechanics problem) at the same location; that is, the cell centers of the developed computational grid. For both the flow and the mechanics problem, we use same unstructured computational grid generated by Delaunay triangulations for the matrix which conforms to the fractures (Shewchuk J. R. 2002).

In the following sections, we give a short review of the discretization methods. Further details on the discretization of the flow problem can be found in Karimi-Fard, et al. (2004) and Sandve, et al. (2012), and details on the discretization of the mechanics problem can be found in Nordbotten (2014), Keilegavlen and Nordbotten (2015) and Ucar et al. (draft manuscript).

3.1.1 Discretization of Flow Problem

For each cell in the computational grid, Ω_i, the mass conservation reads

$$\frac{d}{dt}\int_{\Omega_i} m\, dV + \int_{e_{i,j}} \rho_f w_{\mathbf{n}} dA = \int_{\Omega_i} q\, dV, \quad [18]$$

where $e_{i,j}$ denotes shared boundary between cell Ω_i and nearby cell Ω_j, $\mathbf{w_n}$ is the fluid flux through a surface with normal vector $\mathbf{n}$. The flux $\mathbf{w_n}$ associated with an edge $e_{i,j}$ can further be approximated with considering contributions in the nearby cells,

$$\boldsymbol{w_n} \approx \sum_{j=1}^{n} t_j\, p_j, \quad [19]$$

where n is considered number of contributed nearby cells and t_j is the contribution from the cell j. In this study, the flux terms in equation [19] is approximated by two-point flux approximation (TPFA). The discretization for TPFA considering hybrid grids is described in detail by Karimi-Fard, et al. (2004). To implement TPFA, a computer code based on the Discrete Fracture Matrix module of MATLAB Reservoir Simulation Toolbox (MRST) (Lie 2011) is developed and used to perform numerical simulations on the flow behaviour of fractured.

3.1.2 Discretization of Mechanics Problem

Recently, Nordbotten (2014) proposed a cell centered finite volume method for elastic deformation in porous media as a compatible counterpart to finite volume flow calculations in porous media. In this approach, in order to construct a finite volume formulation, equation [5] was reformulated to obtain a relation for discrete momentum conservation as,

$$\sum_j \int_{e_{i,j}} \mathbf{T} dA + \int_{\Omega_i} \mathbf{f} dV = 0. \quad [20]$$

Further, by defining volume averaged force, $\mathbf{f_i}$, over the cell volume, V, and the surface average stress equation, $\mathbf{T_{i,j}}$, over face, $e_{i,j}$, the equation [20] was rewritten as,

$$\frac{1}{|V|}\sum_j |e_{i,j}|\, \mathbf{T_{i,j}} + \mathbf{f_i} = 0. \quad [21]$$

The surface average stress was further expressed as linear function of displacement, that is,

$$\mathbf{T}_{i,j} = \sum_k t_{i,j,k} \mathbf{u}_k, \quad [22]$$

where $t_{i,j,k}$ are referred as stress weight tensors. The stress weight tensors are then calculated by using information from more than two neighboring cells surrounding the considered cell.

The deformation relations for fracture (equation [9-10]) should be integrated in to the discretization method to model the deformation in fractured porous domain. Therefore, the cells sharing faces with fracture surfaces need a slightly more elaborate approach. Ucar et al. (draft manuscript) have further extended MPSA to include fracture deformation. Following Ucar et al. (draft manuscript), the fracture deformation is implemented through internal boundary conditions in this study.

3.2 Time Discretization

The stress changes are assumed to propagate instantaneously and are, thus, calculated under the quasi-static assumption. In quasi-static mechanics, the time derivative terms appears only in the mass balance equation, equation [1]. The implicit backward Euler scheme is used to approximate the mass accumulation as

$$\partial m/\partial t = (m^{n+1}-m^n)/\delta t, \quad [23]$$

where n denoted current time level, n+1 is next time level and δt is the time step.

3.3 Methods of Solution

The two problems of flow and mechanics are solved in sequence in this study. At the beginning of each time step of the simulation, the flow problem is first solved using implicit time discretization. Next, the Mohr Coulomb criterion is checked for each fracture. For any fracture faces violating the Mohr Coulomb criterion, the shear displacement jump between the fracture surfaces are computed by the joint deformation model (JDM) equations (equations (13)-(16)). Further, the permeability increase of the fracture due to shear dilation is calculated by equation [17]. Subsequently, the estimation of stress redistribution in the domain is calculated by solving for the elastic response of the medium to the fracture slip by using the shear displacement jumps between the fracture surfaces as restrictions on internal boundaries representing the slipped fracture surfaces. Moreover, the Mohr Coulomb criterion is rechecked after the stress redistribution on ground of possible induced additional shear displacements, in what is referred to as ‘shear avalanches’. The Mohr Coulomb criterion check is repeatedly performed until the avalanches stop inducing additional displacements and the next

time step is performed. Figure 2 summarizes the solution strategy for each time step n.

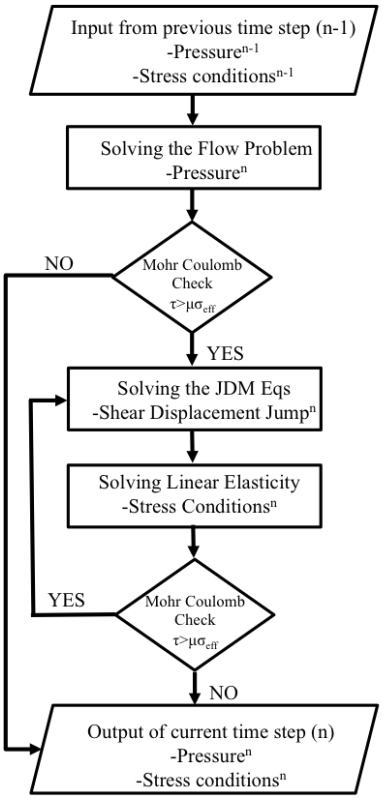

Figure 2: The solution strategy for each time step.

4. NUMERICAL SIMULATIONS

As outlined in the introduction, the aim of this study is to establish an efficient modelling of shear dilation stimulation in fractured rock domains. Moreover, we also wish to underline the effect of permeability in the medium surrounding the explicitly represented fractures. To that end, a two-dimensional 40m x 40m square fractured porous domain is generated. The generated domain, the unstructured mesh used in both flow and mechanics problems and the injection wellbore (shown by red colour) are presented in Figure 3. The fractures are positioned with different angles intentionally to capture the effect of fracture orientation relative to the stress field. The maximum and minimum principle stress directions are parallel to x and y directions respectively. Fluid is injected at a constant pressure below the minimum principal stress, ensuring that tensile fractures would not propagate. The model parameters, presented in Table 1, are configured to loosely resemble reservoir parameters found in the literature.

Only mechanically closed fractures are considered in this study, which means that fracture walls are in contact. Moreover, we do not allow for fracture growth at the tips.

Table I. The properties of fractured geometry.

Porosity	Φ	0.01
Matrix permeability	K	10^{-20} and 10^{-21} m^2
Initial aperture	a_0	10^{-6} m
Viscosity	η	1cP
Maximum principal stress	σ_1	$23.8x10^6$ Pa
Minimum principal stress	σ_2	$14.5x10^6$ Pa
Initial pressure	P_i	$8.7x10^6$ Pa
Fracture shear stiffness	K_s	$5x10^8$ Pa/m
Dilation angle	φ_{dil}	3°
Basic friction angle	φ_{basic}	40°
90% closure stress	σ_{nref}	$20x10^9$ Pa
Lamé's first parameter	μ	$2.4x10^{10}$ Pa
Lamé's second parameter	λ	$2.4x10^{10}$ Pa

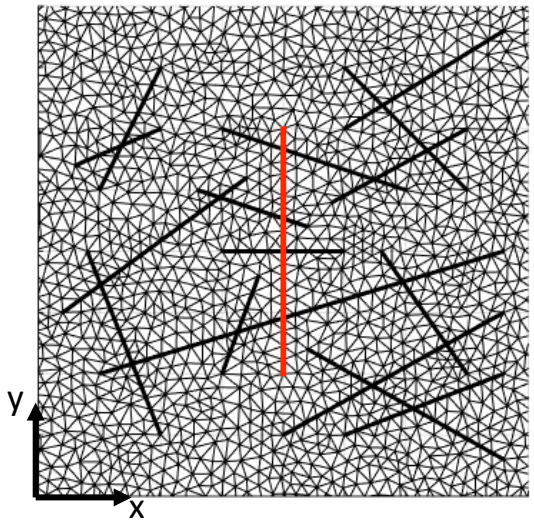

Figure 3: Considered domain with unstructured gridding. The black solid lines represent fracture while the red one represents wellbore.

As an illustrative example, we start with presenting the results of each sequentially coupled physical process. Figure 4 shows the pressure distribution and corresponding induced displacement in the domain after 1000s. The constant pressure injection is provided from the middle of domain that is shown as a red line in Figure 4 (middle and bottom figures). For the sake of illustration, in figures showing mechanical

deformation, fracture faces are marked as white or black depending on whether they have slipped or not. The deformation in the matrix due to the shear displacement jump between face pairs is also shown in Figure 4. The colouring indicates the magnitude of deformation and the arrows show both magnitude and the direction of deformation. As expected, the magnitude of induced slip depends on to the orientation of fractures. The direction of deformation and the magnitude are different across the fracture because of the geometry and the fracture orientation to one another.

We also expect that the face pairs, which have a shear displacement jump, have lower shear stress than the ones next to them. This effect can be seen better at the next time step, shown in Figure 5, which depicts the pressure distribution and corresponding mechanical deformation at time level 2000s. The effect of shear displacement jumps that occurred at the previous time step can be clearly seen in this figure. The shear stresses at the previously slipped face pairs are lower thus they are exposed to lower shear jump. However, the neighbouring face pairs have increased shear stress and consequently have higher shear jumps.

As noted above, the slip of face pairs can cause slip avalanches. This is due to the direct effect of increased shear stress on the neighbouring faces. This effect is displayed in Figure 6, which shows the update from the second mechanics solve at t=2000s. The results show how the slip events cause additional slip events, affecting fracture apertures and displacements in the domain.

To stress the effect of matrix permeability, two numerical simulations are conducted. Both of the simulations have same properties except from the matrix permeability values. First, we present figure 7 that shows the aperture increase at the end of 10 days of constant injection process. As anticipated, the fractures near the injection well have more aperture increase than the others. Moreover, favourably oriented fractures have a larger tendency to slip. As can be seen from the figure, even though the horizontal fracture is exposed high pressure, there is as expected no aperture increase, as the fracture is aligned with a principal stress direction.

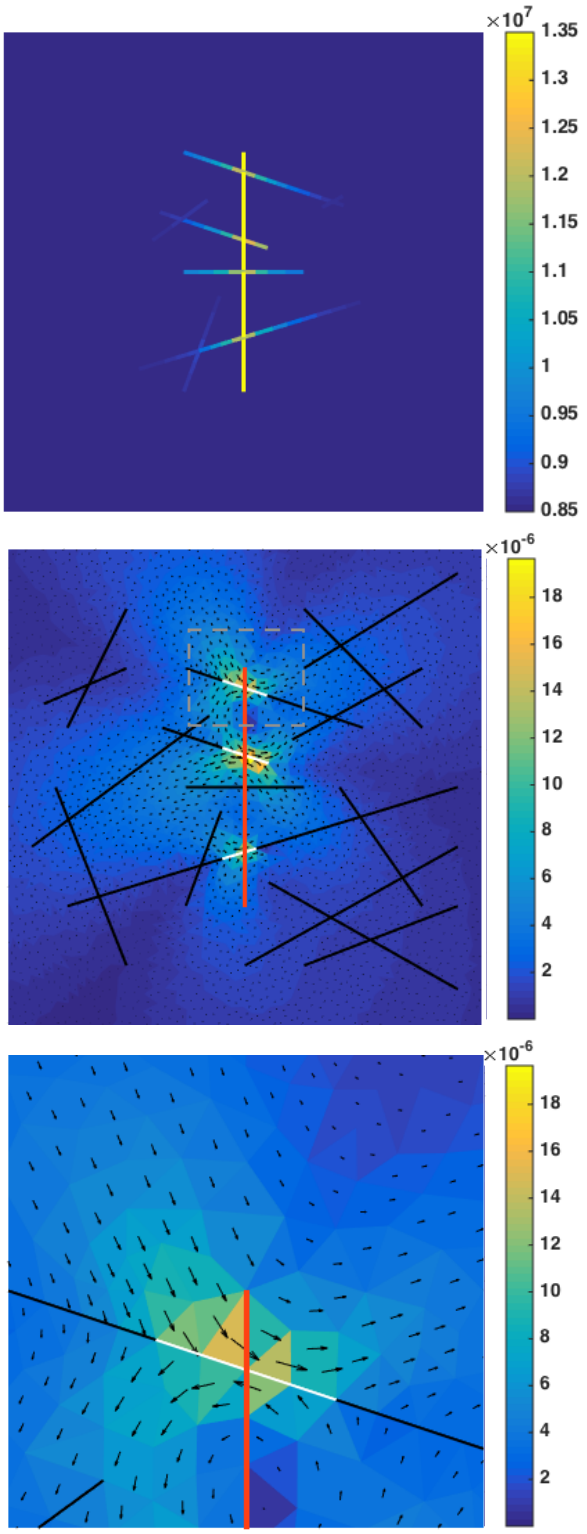

Figure 4: The pressure distribution (top) and induced displacement (middle) after 1000s. To have better inspection of the displacements, the bottom figure shows closer look of grey dashed lined area of the middle figure.

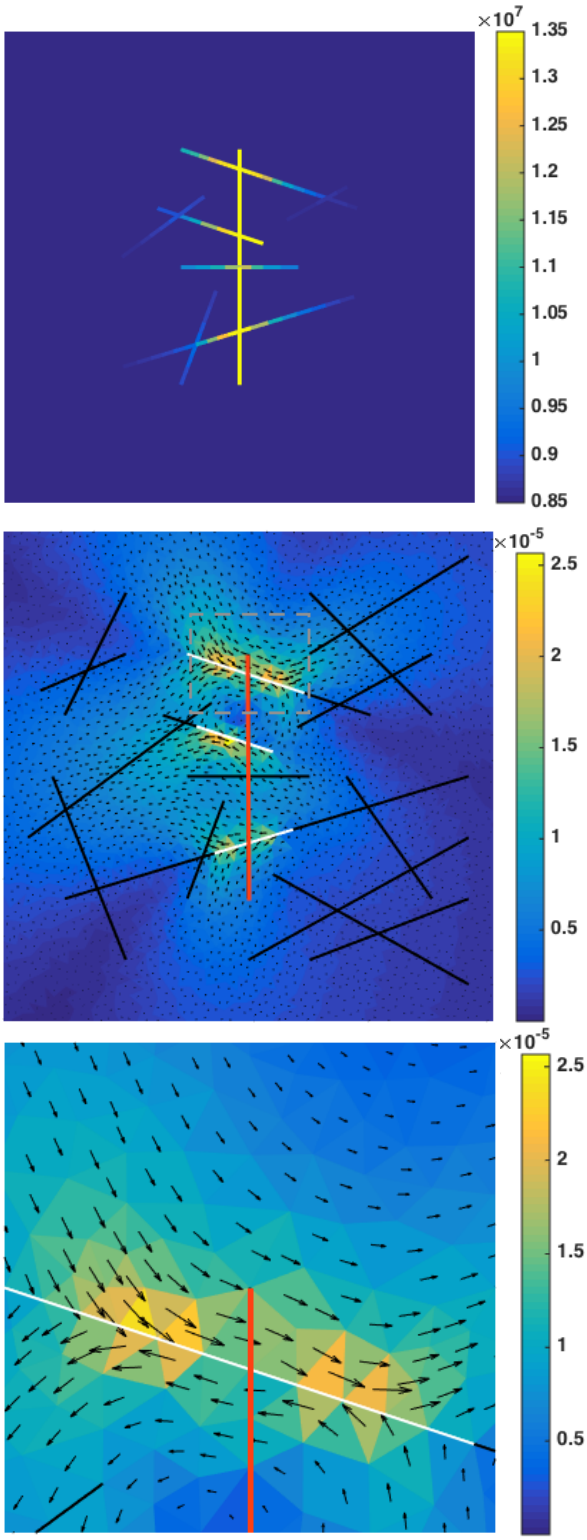

Figure 5: The pressure distribution (top) and induced displacement (middle) after 2000s. To have better inspection of the displacements, the bottom figure shows closer look of grey dashed lined area of the middle figure.

The effect of small-scale fractures can easily be seen by comparing Figure 7 and Figure 8. Figure 7 show the induced apertures when the matrix has permeability of 10^{-21} m^2 whereas Figure 8 shows the induced apertures when the matrix has permeability of 10^{-20} m^2. The difference between two figures is caused by the different pressure distributions in the domain. The flow is more dominated by the fractures when the permeability in the matrix is lower (Figure 7). The low matrix permeability provides high pressures in the fractures by preventing the diffusion of fluid flow in to the matrix. Therefore the fractures are exposed more pressure increase consequently more aperture increase. However, the aperture increase is lower if the permeability is higher in the matrix (Figure 8). In Figure 8, the flow has not diffused yet to the regions far from injection well. Therefore, the aperture increase occurs mainly the area near the injection well. Moreover, because of the higher permeability in the matrix, the flow is less dominated by the fractures.

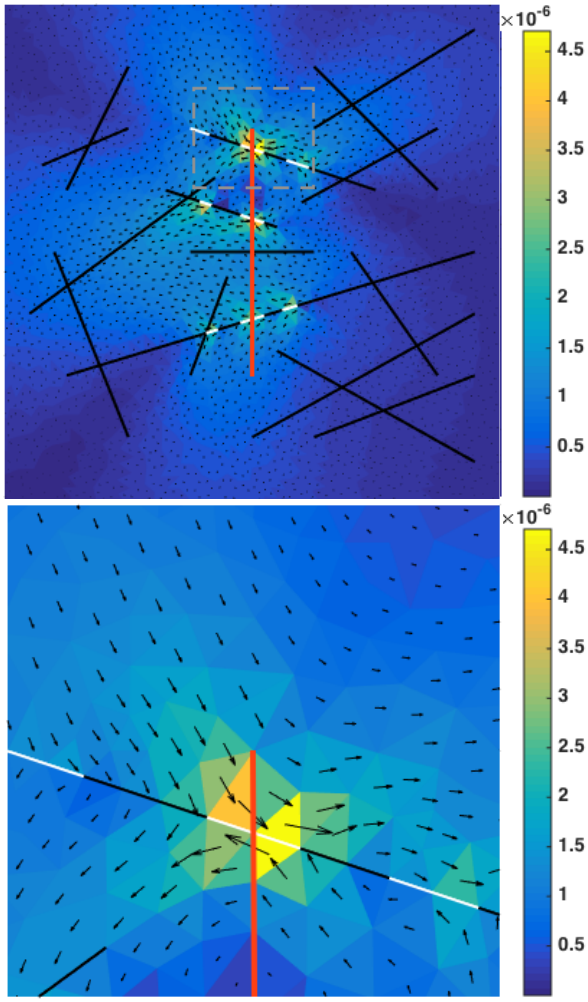

Figure 6: The slip avalanche happens at time step 2000s. The top figure shows the whole domain and the bottom figure shows closer look of grey dashed lined area of the whole domain.

Results of this analysis show that the aperture value and consequently permeability of fractured rock is significantly affected by the permeability of matrix. Therefore, the assumption of zero permeability value for matrix, which commonly is made for several

studies in the literature, may not be precise for prediction of the global flow behaviour of rocks.

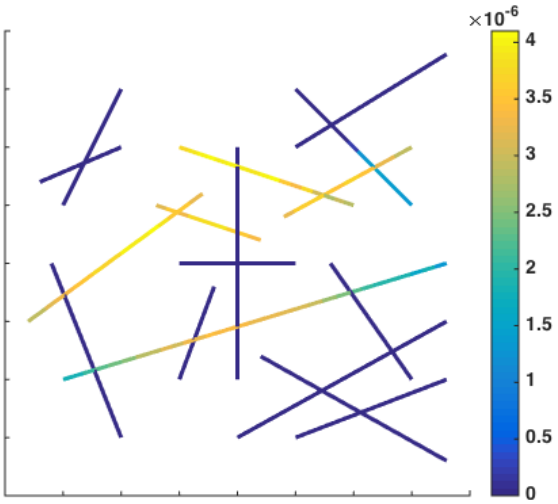

Figure 7: The increase in apertures at the end of 10 days of constant injection process (matrix permeability: 10^{-21} m^2).

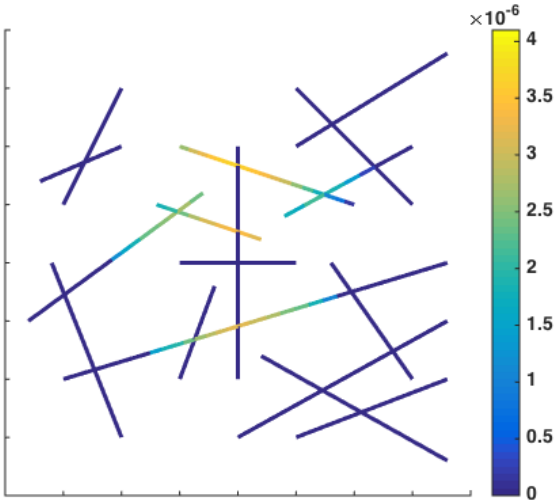

Figure 8: The increase in apertures at the end of 10 days constant injection process (matrix permeability: 10^{-20} m^2).

5. CONCLUDING REMARKS

We have presented a mathematical model and a numerical approach as an effective technique to model shear stimulation in geothermal reservoirs. Our approach couples fluid flow, mechanical deformation and fracture deformation. We presented the results of the sequentially coupled physical processes step by step. The limitations of the current approach are that 1) the elastic deformation is assumed to be quasistatic, 2) the poroelastic and thermoelastic deformations are neglected during the simulations, and, 3) the effect of out of plane dimension is ignored, as only two-dimensional domains are considered. Although MPSA allows for including possible heterogeneity in elastic properties, the elastic properties of the rock were assumed as homogeneous and constant in the current test cases.

Most notably, the (DFM) model for flow used in the current study ensures to investigate the effect of matrix permeability to the global flow behaviour. Consequently, since capturing the effect of the small scale fractures in the matrix influence the precision of the flow approximation, the DFM model avoid inaccurate approximation of permeability increase due to wrong pressure estimates. Moreover, we note that the method can successfully be extended to 3D studies that include heterogeneous elastic properties.

ACKNOWLEDGEMENTS

This work was funded by the Research Council of Norway (grant number 228832/E20).

REFERENCES

Aagaard B., Knepley M. and Williams C.: A domain decomposition approach to implementing fault slip in finite-element models of quasi-static and dynamic crustal deformation. *Journal of Geophysical Research: Solid Earth*,118(6), (2013), 3059-3079.

Barton, N., Bandis S. and Bakhtar K.: Strength, deformation and conductivity coupling of rock joints, *International Journal of Rock Mechanics and Mining Sciences & Geomechanics Abstracts*, 22(3), (1985), 121-140.

Barton, N., and Choubey V.: The shear strength of rock and rock joints in theory and practice. *Rock Mechanics*, 10, (1977), 1–54.

Breede, K., Dzebisashvili K., Liu X. and Falcone G.: A systematic review of enhanced (or engineered) geothermal systems: past, present and future, *Geothermal Energy*, (2013), 1-4.

Bruel, D.: Using the migration of the induced seismicity as a constraint for fractured Hot Dry Rock reservoir modelling, *International Journal of Rock Mechanics and Mining Sciences*, 44(8), (2007), 1106-1117

Chen, Z., Narayan S. P., Yang Z., and Rahman S. S. : An experimental investigation of hydraulic behaviours of fractures and joints in granitic rock, *International Journal of Rock Mechanics and Mining Sciences*, 37, (2000), 1061–1071

Chen, Z., Huan G., Ma Y.: Computational Methods for Multiphase Flows in Porous Media, *Society for Industrial and Applied Mathematics,* (2006)

Crouch S. and Starfield A.: Boundary element methods in solid mechanics, *Allen & Unwin,* London, (1983)

Garipov T. T., Karimi-Fard M., Tchelepi H. A.: Discrete fracture model for coupled flow and geomechanics, *Computational Geosciences*, (2016), 140-160.

Jaeger, J. C., N. G. W. Cook, and R. W. Zimmerman. : Fundamentals of rock mechanics, *Blackwell,* (2007)

Jha B., and Juanes R.: Coupled multiphase flow and poromechanics: A computational model of pore pressure effects on fault slip and earthquake triggering, *Water Resources Research*, 50(5), (2014), 3776-3808.

Jing, Z., Willis-Richards J., Watanabe K., and Hashida T.: A three-dimensional stochastic rock mechanics model of engineered geothermal systems in fractured crystalline rock, *Journal of Geophysical Research*, 105(B10), (2000), 23663-23679

Karimi-Fard M., Durlofsky L., and Aziz K.: An Efficient Discrete-Fracture Model Applicable for General-Purpose Reservoir Simulators, *SPE Journal*, 227-236, (2004)

Keilegavlen E., Nordbotten J. M.: Finite volume methods for elasticity with weak symmetry, arXiv:1512.01042, (2015)

Kim J., Tchelepi H. and Juanes R.: Stability, Accuracy, and Efficiency of Sequential Methods for Coupled Flow and Geomechanics, *SPE Journal,* 16(02), (2011), 249-262.

Lie K., Krogstad S., Ligaarden I., Natvig J., Nilsen H. and Skaflestad B.: Open-source MATLAB implementation of consistent discretisations on complex grids, *Computational Geosciences,* 16(2), (2011), 297-322.

Min, K. B., Rutqvist J., Tsang C.-F., and Jing L.: Stress-dependent permeability of fractured rock masses: A numerical study, *International Journal of Rock Mechanics and Mining Sciences*, 41, (2004), 1191–1210

Murphy, H. D. and M. C. Fehler,: Hydraulic fracturing of jointed formations, SPE 14088, *International Meeting on Petroleum Engineering*, Beijing, China, (1986)

McClure M. W., and Horne R. N.: Investigation of injection- induced seismicity using a coupled fluid flow and rate/state friction model, *Geophysics*, 76 (6), (2011), WC181–WC198,

McClure M. W., and Horne R. N.: An investigation of stimulation mechanisms in Enhanced Geothermal Systems. *International Journal of Rock Mechanics and Mining Sciences*, 72:242, (2014), 260

Norbeck J., McClure M., Lo J., and Horne R. N.: An embedded fracture modeling framework for simulation of hydraulic fracturing and shear stimulation, *Computational Geosciences,* 20(1), (2016), 1-18.

Nordbotten J.: Cell-centered finite volume discretizations for deformable porous media, *International Journal for Numerical Methods in Engineering*, 100(6), (2014), 399-418.

Olsson R, and Barton N.: An improved model for hydromechanical coupling during shearing of rock joints, *International Journal of Rock Mechanics and Mining Sciences*, 38, (2001), 317–239

Pine R. J., and Batchelor A. S.: Downward migration of shearing in jointed rock during hydraulic injections, *International Journal of Rock Mechanics and Mining Sciences & Geomechanics Abstracts,* 21(5), (1984), 249-263,

Rahman M. K., Hossain M. M. and Rahman S. S. A Shear-Dilation-Based Model for Evaluation of Hydraulically Stimulated Naturally Fractured Reservoirs, *International Journal for Numerical and Analytical Methods in Geomechanics*, 26(5),, (2002), 469-497

Sandve T., Berre I., and J.M. Nordbotten.: An efficient Multi-Point Flux Approximation based approarch for Discrete Fracture Matrix Simulations, *Journal of Computational Physics*, 231(9), (2012), 3784-3800

Shewchuk J. R.: Delaunay Refinement Algorithms for Triangular Mesh Generation, *Computational Geometry: Theory and Applications* 22(1-3), 2002, 21-74

Tao Q., Ghassemi A., and Ehlig-Economides C.: A fully coupled method to model fracture permeability change in naturally fractured reservoirs. *International Journal of Rock Mechanics and Mining Sciences*. 48(2), (2011), 259-268.

Tezuka K., Tamagawa T., and Watanabe K.: Numerical Simulation of Hydraulic Shearing in Fractured Reservoir, *Proceeding World Geothermal Congress*, (2005).

Ucar E., Keilegavlen E, Berre I. and Nordbotten J. M.: Finite Volume Discretization for Deformation of Fractured Media, manuscript is in preparation for *Computational Geosciences*, (2016)

Willis-Richards J., Watanabe K., and Takahashi H.: Progress toward a stochastic rock mechanics model of engineered geothermal systems, *Journal of Geophysical Research*, 101(B8), (1996), 17481-17496

Zhang Z., Crosby D., Akgun F., Khurana A., and Rahman S.: Investigation of the Factors Influencing Hydraulic Fracture Initiation in Highly Stressed Formations. *SPE Asia Pacific Oil and Gas Conference and Exhibition*, Kuala Lumpur, Malaysiaaysiar: Society of Petroleum Engineers. (1997)

Zimmerman R. W., and Bodvarsson G. S.: Hydraulic conductivity of rock fractures, *Transport in Porous Media*, 23(1), (1996), 1–30.